RSC Advances

PAPER

View Article Online
View Journal | View Issue

Cite this: *RSC Adv.*, 2023, **13**, 27501

Synthesis, characterization, molecular docking, and antimicrobial activities of dinuclear nickel(II), palladium(II), and platinum(IV) complexes†

Reem M. A. Ebrahim, *[ad] Abubakar Abdelbagi,[b] Yousif Sulfab,*[c] Omer Abdalla Ahmed Hamdi,[c] Samah A. Shokri[b] and Elmugdad A. Ali[d]

Received 15th July 2023
Accepted 25th August 2023

DOI: 10.1039/d3ra04768g

rsc.li/rsc-advances

New nickel(II), palladium(II), and platinum(IV) complexes were synthesized by reacting the metal ions with benzidinedioxime in a 1 : 1 mole ratio. The CHN elemental analysis, spectroscopic analyses, and powder X-ray diffraction (PXRD) results showed that two Ni(II) and two Pd(II) ions coordinated to two benzidinedioxime ligands *via* the nitrogen atoms of both oxime groups and the two azomethine nitrogen atoms. In the case of the dinuclear platinum(IV) complex, however, each Pt(IV) is coordinated with the two oxygen atoms of the oxime group and the two azomethine nitrogen atoms of the ligand. Both elemental analyses and PXRD indicated that the complex ions of Ni(II) and Pt(IV) have distorted octahedral geometry, whereas Pd(II) has a square planar geometry. Molecular docking studies showed that the nickel(II) complex is the most potent dual DHPS/DHFR bacterial inhibitor. The receptor of the DHPS enzyme (3ZTE) showed the best interaction with the nickel(II) complex when compared to a receptor of the DHFR enzyme (3FRB). All the synthesized complexes and ligand exhibited significant results against *PS. Aeruginous* than their corresponding SMX–TMP drug. Among the three synthesized complexes, the nickel(II) complex possessed the highest antimicrobial activities against tested microorganisms.

Introduction

Schiff base ligands have played essential roles as excellent chelating agents due to a lone pair of electrons in an sp^2 hybridized orbital of the nitrogen atom in the azomethine group.[1–3] Schiff base complexes have different physical and chemical properties and pharmacological activities than their corresponding ligands. The variation of properties of their complexes depends on the type of metal used.[4–7]

In recent years, Schiff base transition metal complexes played essential roles in different fields such as agriculture,[8–10] pharmaceutics,[11–13] and industry.[14,15] They have biological properties, such as antibacterial, antifungal, anticancer, and herbicidal applications.[16–20] The chemical structural and functional groups of Schiff base ligands play an essential role in the mechanism of several enzymes. For example, aminotransferase enzymes use pyridoxal phosphate as a cofactor.[21]

Dinuclear Schiff base transition metal complexes comprise two transition metal ions in the same molecular entity.[22–24] The magnetic properties of dinuclear complexes can differ significantly from those of mononuclear complexes. These new properties depend on the nature and magnetic interaction between the metal ions through the bridging ligands.[22–24] Several dinuclear complexes having N_4O_4 Schiff-base ligands have been reported, and the antibacterial activity of these complexes screened against Gram-positive and Gram-negative strains.[25–27] Compared to standard drugs, the complexes most potent activity was observed against all tested strains.[27–30]

The Sulfamethoxazole–Trimethoprim (SMX–TMP) antibiotic drug is an inhibitor of two enzyme families involved in synthesizing tetrahydrofolate (THF). These are dihydropteroate synthase (DHPS) and dihydrofolate reductase (DHFR). Sulfamethoxazole (SMX) binds to bacterial dihydropteroate synthase (DHPS) to the conversion of *para*-aminobenzoic acid (PABA) to dihydropteroate (DHP) in the process of THF formation. DHPS inhibition leads to defective thymidine biosynthesis and slows or blocks folic acid biosynthesis.[31,32] The second enzyme is Dihydrofolate Reductase (DHFR) is a vital antibiotic target in folic acid biosynthesis.[33] It catalyzes the production of nicotinamide adenine dinucleotide phosphate (NADPH) by the reduction of dihydrofolate (DHF) to tetrahydrofolate (THF).[32,34,35] Trimethoprim (TMP) is a drug used to treat urinary tract infections (UTIs). It inhibits bacterial DHFR.[32,36] TMP is highly effective in *S. aureus* DHFR (SaDHFR) than in human DHFR, which leads to preferential inhibition of

[a]*Biotechnology Department, Africa City of Technology, Khartoum, Sudan. E-mail: reemaaboalsoud@gmail.com*

[b]*Pharmaceutical Microbiology Department, Faculty of Pharmacy, Al-Neelain University, Khartoum, Sudan*

[c]*Chemistry Department, Faculty of Science and Technology, Al-Neelain University, Khartoum, Sudan. E-mail: yousifsulfab@yahoo.com*

[d]*Chemistry Department, Faculty of Science, Sudan University of Science and Technology, Khartoum, Sudan*

† Electronic supplementary information (ESI) available. See DOI: https://doi.org/10.1039/d3ra04768g

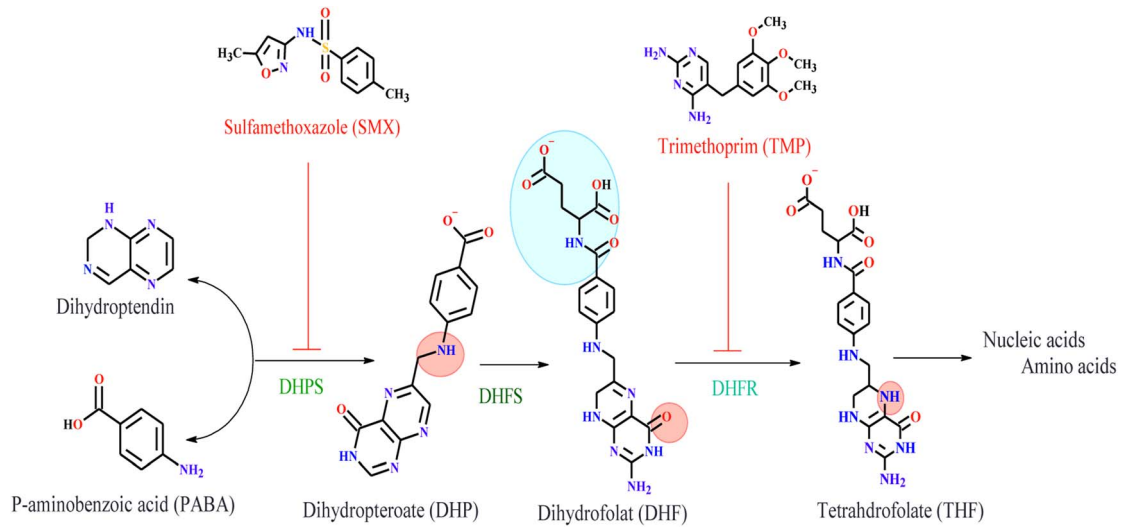

Fig. 1 Folic acid biosynthesis pathway in bacteria. The key enzymes involved in folic acid metabolism were labeled in green, dark green, and turquoise, while antibiotics that inhibit them are shown in red.

bacterial folic acid synthesis.[31,32] The key enzymes involved in bacterial folic acid biosynthesis and the antibiotics that inhibit them are shown in Fig. 1. The dual targeting of two enzymes made SMX–TMP an excellent choice for treating bacterial infections. However, this has resulted in the development of antimicrobial resistance,[32] encouraging us to synthesize new compounds containing dinuclear metal ions and test them as bacterial inhibitors for DHPS and DHFR enzymes.

Materials and methods

Materials

Benzidine (99%, Riedel-de-Haen AG, Germany), diacetylmonoxime (99%, Trust Chemical Laboratories, India). Platinum(IV) chloride (assay = 99.99%, Onyxment, Poland). Nickel(II) chloride hexahydrate (assay = 98.0%, Loba Chemie, Spain). Palladium(II) acetate (assay = 98%, Sigma-Aldrich, Germany). Ethanol (99.9%, Duksan, Germany). Methanol (assay = 99.8%, Sigma-Aldrich, Germany). Diethyl ether (97.5%, Alpha Chemika, India). Dimethyl sulphoxide (99.9, Alpha Chemika, India). Glacial acetic acid (85%, Alpha Chemika, India) were used as received.

Synthesis of the benzidinedioxime ligand (N2,N2′-biylbis(N3-hydroxybutane-2,3-diimine))

Benzidine (2.00 g, 10 mmol) was dissolved in 50 mL of absolute hot ethanol, and 2,4 butene-dione monoxime (2.22 g, 20 mmol) was dissolved in 20 mL of absolute ethanol. A few drops of glacial acetic acid were added to the mixture. The mixture was refluxed by stirring for 8 hours. The precipitate was filtrated, washed with cold ethanol and ether, and left to dry in the air.

Synthesis of the metal complexes

The metal complexes were prepared by adding a hot solution of the appropriate metal salt (2.5 mmol) in ethanol to a hot benzidinedioxime ligand (2.5 mmol) solution. The resulting mixture was stirred under reflux for 20 hours, and the complexes precipitated. The precipitate was filtered off and washed with cold ethanol and diethyl ether several times.

Elemental analysis measurement

The elemental analyses of benzidinedioxime and its complexes were determined using Flash EA 1112 CHN.

^{1}H-Nuclear magnetic resonance (^{1}HNMR)

The ^{1}H NMR spectrum was obtained for the dioxime benzidine and complexes solution in DMSO D_6 (0.05 mM) using a Bruker DPX 250 and 300 MHz spectrometer. Standard pulse sequences were used for the ^{1}H one-bond and long-range HMBC spectra.

Electronic properties

The electronic spectra were obtained using a Shimadzu 160 UV-visible spectrophotometer in the range (of 200–1000 nm) using a quartz cell of 1.0 cm length with a concentration of 1.43 mmol L^{-1} of samples in dimethyl sulfoxide at 25 °C.

Powder X-ray diffraction (PXRD)

The powders' crystalline phases and unit cell parameters were determined by PXRD using a Shimadzu 7000 X-ray diffractometer. At room temperature, data were collected for a 2θ range of 20–80° at a step size of 0.02 and a 5 seconds count time.

Molecular docking

The molecular docking studies were carried out using Molecular Operating Environment (MOE 2014). All the minimizations were performed with MOE until an RMSD gradient of 0.01 kcal mol^{-1} $Å^{-1}$ with an MMFF94X force field was achieved, and the partial charges were automatically calculated. Docking simulations were performed using the crystal structure of DHPS enzyme (PDB ID : 3TYE) in complex to XTZ and the crystal

structure of DHFR enzyme (PDB ID : 3FRB) in complex to TOP, which was obtained from Protein Data Bank. Finally, the optimized poses were ranked using the London DG free-energy estimates. Docking poses were visually inspected, and interactions with binding pocket residues were analyzed.

Antimicrobial activity

The antimicrobial potency of 10 mg mL^{-1} of synthesized compounds, trimethoprim sulfumethaxol, and Gentamycin was evaluated by cup plate method according to Seeley *et al.* 1975.[37] Using many standards and isolated microorganisms, two Gram-positive bacteria: *Staphylococcus aureus*, ATCC25923, and *Bacillus subtilis* MCTC8236. Four Gram negative bacteria, *Pseudomonas aeruginosa* ATCC9017, *Proteus Vulgaris* ATCC6380, *Salmonella typhimurium* (isolate), and *Escherichia coli* ATCC25922 and fungi as candid albicans ATCC4430373. All strains were provided by the National Research Centre (NRC); in Khartoum, Sudan.

Results and discussion

Synthesis

The yield of benzidinedioxime (3Z,2′E,3′Z)-N2,N2′-biylbis (N3-hydroxybutane-2,3-diimine) is found to be 73% and has a melting point of 242 °C. Benzidinedioxime is soluble in ethanol and DMSO.

The nickel(II), palladium(II), and platinum(IV) complexes are intensely colored and stable in the solid form. Their m.p. is >360 °C. The yield of the complex of nickel(II), palladium(II), and platinum(IV) were found to be 58.0%, 83.64%, and 85.15%, respectively. All complexes are partially soluble in ethanol and are soluble in DMSO.

Fourier transform-infrared (FT-IR) analyses of ligand and complexes

FT-IR spectroscopy measurements were performed to examine the functional groups present in the ligand in the range of 4000 cm^{-1} to 400 cm^{-1}.

The FT-IR spectra of the benzidinedioxime are shown in Table 1. This spectrum confirms the proposed structure. After the condensation reaction of benzidine, the new peak at 1616 cm^{-1} indicating imine CH═N bond appears; these assignments are in good agreement with theoretical and literature data.[38–41]

Elemental analysis measurement

The H, C, and N percentages in the ligand and complexes have been determined by CHN elemental analyzer. The results are within the accepted ±5.0% error margin. The complexes have 1 : 1 metal to ligand stoichiometry. The proposed formulae and elemental analysis data of the ligand and complexes are shown in Table 2.

Nuclear magnetic resonance

Benzidinedioxime. Aromatic protons of the benzene rings appeared as a quartet signal around 6.52–6.8 ppm and 7.14–7.63 ppm in a different environment.[42–44] The protons of the oxime group emerged as a doublet signal at 11.82 ppm Fig. 1ESI.†

Complexes. The ^{1}H NMR spectrum of the complexes of bis-(benzidinedioxime) of Pd(II), Pt(IV), and Ni(II) scanned in DMSO-d6 showed the peak at the chemical shift range from 1.5 to 2.24 ppm due to twelve methyl protons in different environments. All protons of phenyl groups of complexes shown in the closed chemical shift range of benzidinedioxime ligand (7.0–8.0) except for the platinum(IV) complex, which appeared an increase in the chemical shift of protons of phenyl groups at chemical shift value 9, and that due of high electrons density of platinum metal[45–47] Fig. 2ESI–4.†

The palladium(II) complex appears to have a high-intensity peak for protons of phenyl groups as compared to the complexes of nickel(II) and platinum(IV) that due to the different shapes of the crystal, hydrogen bonds, and symmetric and

Table 2 Experimental and calculation of C, H, and N in ligand and complexes

	Experimental percentage (%)			Calculation percentage (%)		
Compounds	C	H	N	C	H	N
$C_{20}H_{22}N_4O_2$	70.77	6.43	15.14	68.5	6.29	16.00
$[Ni_2(C_{20}H_{22}N_4O_2)_2](Cl)_4\ (H_2O)_6$	46.85	5.47	10.97	48.29	5.63	11.27
$Pd_2(C_{20}H_{22}N_4O_2)_2(CH_3CO_2)_4$	53.92	5.32	10.12	53.49	5.20	10.4
$Pt_2(C_{20}H_{20}N_4O_2)_2(Cl_4)(H_2O)_4$	40.08	4.12	8.90	40.10	4.01	9.36

Table 1 Characteristic infrared absorption frequencies of benzidinedioxime, the complex of Ni(II), the complex of Pd(II), and the complex of Pt(IV)

Benzidinedioxime	Complex of Ni(II)	Complex of Pd(II)	Complex of Pt(IV)	
Wave number (cm^{-1})	Wave number (cm^{-1})	Wave number (cm^{-1})	Wave number (cm^{-1})	Functional groups
3365, 3296	3433, 3336	3329, 3199	—	O–H stretching vibrations of the oxime group
2775	3032	3043	3198	Stretching vibrations of saturated C–H
1617	1612	1619	1607	C═N stretching vibrations of imine
1463	1489	1567	1496	C–H bending vibration
1362, 1258, 1121	1378, 1288, 1233	1499, 1381, 1278	1404, 1404, 1187	C═C stretching vibrations of the aromatic ring
1017	1173	1204	1013	C–C stretching vibration
970	824	820	821	C–N stretching vibration

asymmetric structure of the complexes.[48] The change of chemical shift value and intensity of protons of aromatic complexes aromatic rings indicate the formation of coordinate bonds between para-imine groups with metals. The disappearance of protons of oxime groups indicates the coordination of deportation of the oxime groups by metal ions or the formation of hydrogen bonds.

Powder X-ray diffraction

The crystal structure of complexes bis-benzidinedioxime was determined by powder X-ray diffraction. Pattern peaks of bis-benzidinedioxime complexes display that almost all the crystals were grown in the same phase. The crystals obtained from complexes are shown to be weak diffracting and fail to provide high-resolution reflection data. As a consequence of Fig. 5ESI,† only partial structure determination was possible. The bond length and angles' accuracy has determined the crystal structure's quality. The brood peak indicated a small crystallization size in the nano-crystalline scale range.

The crystal properties of benzidinedioxime and dinuclear complexes were reported in Table 3. The metal center of palladium (53) has little distortion of square planar geometry, while palladium (54) has a high distortion of square planar geometry.

The atoms central of nickel(II) and platinum(IV) have slight distortion octahedral coordination geometry defined by two chelating atoms (benzidinedioxime ligand) and two monodentate ligands (di aqua ligands) at a complex of nickel(II) and dichloro ligands at a complex of platinum shown in Fig. 2. The selected bonds and angles of the complex of Ni(II), Pd(II), and Pt(IV) are represented in Tables 4 and 5, respectively.

Electronic properties of ligand and complexes

Ligand and complexes scanned in the range 200–1000 nm.

Table 3 Crystal properties of benzidinedioxime, bis-benzidinedioxime nickel(II), bis-benzidinedioxime palladium(II), and bis-benzidinedioxime platinum(IV) were solved by using EXPO 2014 software

Properties	Benzidinedioxime	Bis-benzidinedioxime nickel(II)	Bis-bezidinedioxime palladium(II)	Bis-benzidinedioxime platinum(IV)
Space group	*P*1 (1)	*P* 21 3	*P* -1	*P* 41 3 2
Symmetry operations	Centrosymmetric	Non-centrosymmetric	Centrosymmetric	Non-centrosymmetric
Lattice type	Triclinic	Cubic	Triclinic	Cubic
Cell volume (°A^3)	983.920	1022.021	1942.981	995.875
Alpha	98.853	90.000	90.705	90.000
Beta	91.032	90.000	93.634	90.000
Gamma	88.809	90.000	101.998	90.000
A/°A	9.96474	10.073	8.175	9.986
B/°A	9.84346	10.073	14.844	9.986
C/°A	992 847	10.073	16.408	9.986

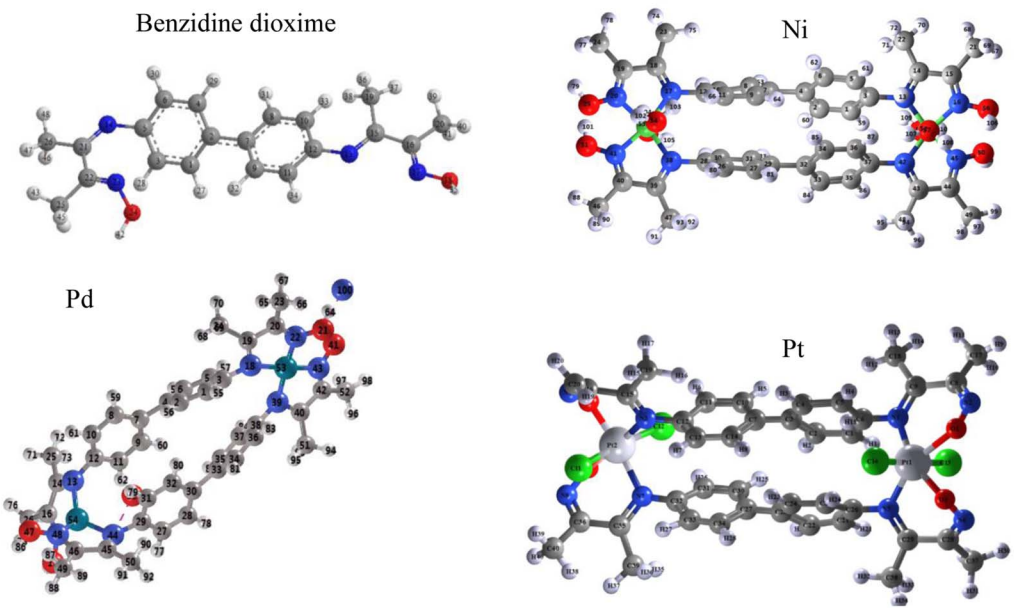

Fig. 2 PXRD crystal structure of benzidinedioxime, bis-benzidinedioxime nickel(II), bis-benzidinedioxime palladium(II), and bis-benzidinedioxime platinum(IV).

Table 4 Selected bonds distances of complex of nickel(II), palladium(II) and platinum(IV)

Atom	Bond distance (°A)	Atom	Bond distance (°A)	Atom	Bond distance (°A)
Ni52-O57	1.86	Pd53-N22	1.76	N17-Pt54	2.03
Ni52-O58	1.86	Pd53-N39	1.81	N44-Pt54	2.03
Ni53-O54	1.86	Pd53-N43	1.77	N7-Pt27	1.93
Ni53-O55	1.86	Pd53-N18	1.81	N34-Pt27	2.15
N13-Ni52	1.83	Pd54-N13	2.026	O21-Pt27	1.93
N16-Ni52	1.82	Pd54-N17	2.008	O48-Pt27	1.86
N42-Ni52	1.83	Pd54-N44	2.032	O26-Pt54	1.87
N45-Ni52	1.82	Pd54-N48	2.015	O53-Pt54	1.87
N41-Ni53	1.82			Pt54-Cl55	2.42
N17-Ni53	1.91			Pt54-Cl56	2.42
N20-Ni53	1.89			Pt27-Cl57	2.34
N38-Ni53	1.91			Pt27-Cl58	2.39

Table 5 Selected bonds angles of complex of nickel(II), palladium(II) and platinum(IV)

Atom	Bond angles (°A^3)	Atom	Bond angles (°A^3)	Atom	Bond angles (°A^3)
Ni52-N16-O56	125.01	N13-Pd54-N44	125.74	N7-Pt27-O21	86.48
N16-Ni52-N42	160.31	N13-Pd54-N48	127.76	N7-Pt27-N34	103.93
N16-Ni52-N5	88.99	N17-Pd54-N44	126.59	N7-Pt27-O48	171.57
N16-Ni52-O57	85.83	N17-Pd54-N48	109.67	N7-Pt27-Cl57	81.12
N16-Ni52-O58	101.76	N18-Pd53-N39	91.64	N7-Pt27-Cl58	92.14
N17-Ni53-N20	82.8	N18-Pd53-N43	174.05	N17-Pt54-O26	88.39
N17-Ni53-N38	111.98	N22-Pd53-N39	174.15	N17-Pt54-Cl55	85.86
N17-Ni53-N41	162.69	N22-Pd53-N43	90.69	N17-Pt54-Cl56	89.54
N17-Ni53-O54	92.76	N13-Pd54-N17	85.96	O21-Pt27-N34	167.65
N17-Ni53-O55	79.98	N18-Pd53-N22	89.45	O21-Pt27-O48	85.73
N41-Ni53-O54	99.12	N39-Pd53-N43	88.82	O21-Pt27-Cl57	91.95
N41-Ni53-O55	90.41	N44-Pd54-N48	84.98	O21-Pt27-Cl58	96.16
N42-Ni52-N45	83.8			N17-Pt54-N44	97.01
N42-Ni52-O57	77.69			N17-Pt54-O53	174.61
N52-Ni52-O58	96.0			O26-Pt54-N44	172.24
N20-Ni53-N38	162.24			O26-Pt54-O53	87.5
N20-Ni53-N41	84.57			O26-Pt54-Cl55	92.58
N20-Ni53-O54	90.28			O26-Pt54-Cl56	91.75
N20-Ni53-O55	99.15			N34-Pt27-O48	83.45
N38-Ni53-N41	82.72			N34-Pt27-Cl57	83.27
N38-Ni53-O54	79.57			N34-Pt27-Cl58	90.15
N38-Ni53-O55	93.32			O48-Pt27-Cl57	95.91
N45-Ni52-O57	101.27			O48-Pt27-Cl58	91.91
N45-Ni52-O58	85.96			N44-Pt54-O53	86.75
O57-Ni52-O58	169.69			N44-Pt54-Cl55	82.3
N13-Ni52-N16	84.25			N44-Pt54-Cl56	93.86
N13-Ni52-N2	108.05			Cl57-Pt27-Cl58	169.13
N13-Ni52-N45	160.5			O53-Pt54-Cl55	90.85
N13-Ni52-O57	96.48			O53-Pt54-Cl56	94.07
N13-Ni52-O58	77.58			Cl55-Pt54-Cl56	173.59

The spectrum shows many peaks due to electronic, vibration, and rotation transitions. All compounds have a strong peak at 300 nm indicating high electronics transition in the UV region Fig. 3. The spectra showed two peaks at around 300–350 nm due to $n \rightarrow \sigma^*$ and $n \rightarrow \pi^*$ electronic transitions. The absorption in the 400 nm is due to $\pi \rightarrow \pi^*$ electronic transition of the unsaturated conjugated compound Fig. 3.

Molecular docking

Molecular docking studies using a crystal structure of DHPS (PDB ID : 3TYE) and DHFR (PDB ID : 3FRB) obtained from the Protein Data Bank server. The result demonstrated that the benzidinedioxime, bis-benzidinedioxime nickel(II), bis-benzidinedioxime palladium(II), and bis-benzidinedioxime platinum(IV) have higher activity and lower root mean square

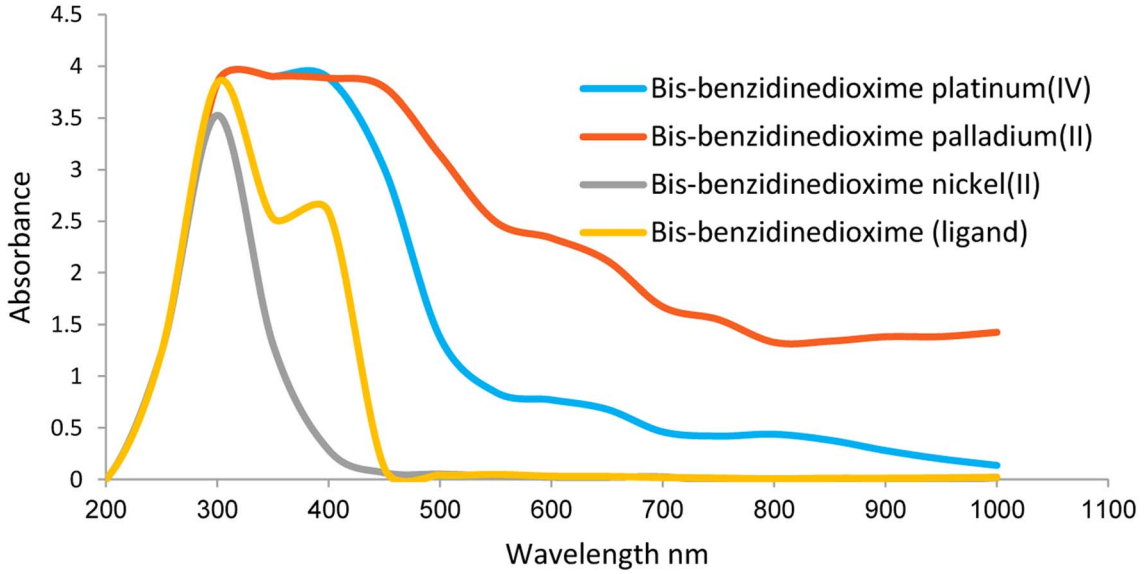

Fig. 3 Electronic properties of benzidinedioxime, bis-benzidinedioxime nickel(II), bis benzidinedioxime palladium(II) and bis-benzidinedioxime platinum(IV).

deviation (RMSD) value against DHFR than DHPS, as shown in Table 6. Furthermore, the bis-benzidinedioxime nickel(II) complex showed the best potent inhibitor against both enzymes.

Fig. 4 shows 2D interactions of the co-crystallized Trimethoprim (TMP) ligand and complexes compound within the active site of DHFR. 2D interaction of the TMP ligand displays that the two amino groups at the pyrimidine create hydrogen bond donors with Asp 27 and Leu 5. Thr 46, Val 31, and Ser 49 are attached to the TMP ligand by Vander Waal interaction. The closed contour indicated the lower solvent exposure to terminal atoms Fig. 4(A).

Fig. 4B and 5 show that bis-benzidinedioxime nickel(II) can fit into a DHFR pocket with four hydrogen bond donors. One of the donor hydrogen bonds was created between the methyl group and Asp 120. In contrast, three hydrogen bond donors formed between Thr121, Asn 18, and Asp 27 with the water molecular, which bonded by a coordinated bond with the transition metal (nickel(II)). The acceptor hydrogen bond is produced amongst the oxygen atom at the aqua ligand with Asp 120. The imine group bonded by an ionic bond with Asp 27. Arene–H connected with bis-benzidinedioxime nickel(II) with Phe 92. Additionally, Vander Waal interactions formed between complex and hydrophobic residues. Losing the contour around a compound indicated that the intermediate solvent interacted with terminal atoms. The docking revealed that the bis-benzidinediooxime of palladium(II) interacts with Asn 18, and Asp 27 amino acid residues of DHFR enzyme *via* donor hydrogen bonds, which formed between the phenyl ring and hydroxyl group respectively. Arene–H linked with phenyl ring and Thr 46 as well as many of Vander Waal interactions formed between Asn 18, Glu 17, Thr 46, Lys 45, Gly 94, Leu 20, Ser 49. Phe 16, Ile 50, Leu 28, Phe 92, Val 31, Val 6, Ala 7, Ile 14, Thr 121 and Asp 120 Fig. 6ESI(D).† Missing the contour around

Table 6 Binding energy and RMSD-refine of dock benzidinedioxime and complexes with 3FRB (DHFR enzyme) and 3TYE (DHPS enzyme)

	Binding energy (*S*) and RMSD- refine of dock benzidinedioxime and complexes with 3FRB (DHFR enzyme)		Binding energy (*S*) and RMSD- refine of dock benzidinedioxime and complexes with 3TYE (DHBS enzyme)	
Compounds	*S*	RMSD-refine	*S*	RMSD-refine
Bis-benzidinedioxime nickel(II)	−21.23	1.874	−22.00	1.779
Bis-benzidinedioxime palladium(II)	−18.80	1.694	−19.16	2.952
Bis-benzidinedioxime platinum(IV)	−16.13	1.286	−14.49	1.559
Benzidinedioxime	−10.47	1.340	−9.386	1.346
XTZ	—	—	−14.054	1.608
TMP	−11.27	1.217	—	—
Gentamycin	−17.63	1.894	−15.91	1.749

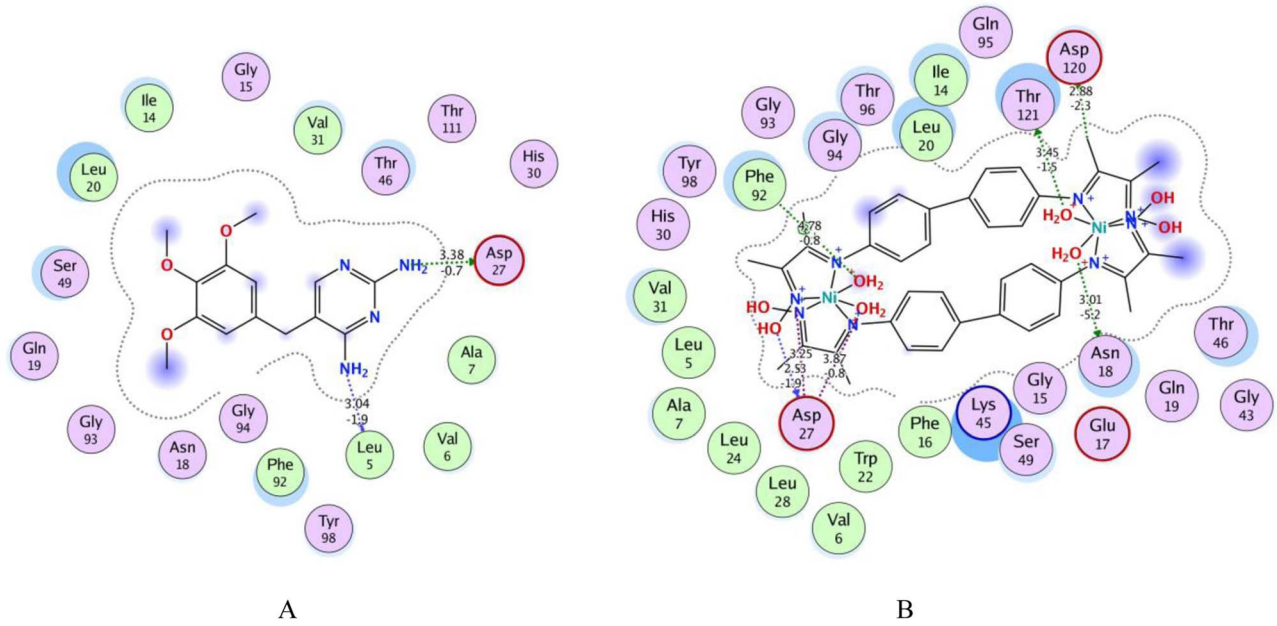

Fig. 4 2D interaction of TMP ligand, and bis-benzidinedioxime complexes with DHFR pocket, (A) 2D interaction of the TMP ligand with DHFR pocket (B) 2D interaction of complex of nickel(II) with DHFR pocket respectively.

a compound indicated that the intermediate solvent was exposed to terminal atoms. The bis-benzidinedioxime platinum(IV) interacts with the active site *via* an ionic bond that is formed between the imine group and Asp 120 and a donor hydrogen bond between the benzene ring and chloride ion with Asp 120 and Ile 14 respectively. Arene–H is linked between the benzene ring and Asn 18, and another arene–H is coupled between the alkyl group and Phe 92. The platinum(IV) also provides a molecular bulk necessary for Vander Waal interactions with Lys 45, Asp 120, Thr 121, Asn 18, Ser 49, Ile 14, Leu 20, Ile 50, Leu 28, Tyr 98, Phe 92, Val 31, Ala 7, Gly 94, Thr 96, Gln 95 and Thr 46 Fig. 6ESI(E).† Losing the contour around a compound indicated that the intermediate solvent interacted with terminal atoms. The oxime group of benzidinedioxime has formed a donor hydrogen bond with Asp 120 furthermore, Vander Waal interactions formed between benzidinedioxime and Thr 121, Ile 14, Thr 46, Ser 49, Ile 50, Leu 28, Val 31, Leu 54, Phe 92, Leu 20, and Asn 18 Fig. 6ESI(F).† Losing the contour around a compound indicated that the intermediate solvent interacted with terminal atoms.

4-[(2-amino-4-oxo-3,4,7,8-tetrahydropteridin-6-yl) methyl] amino-N-(1,3-thiazol-2-yl) benzenesulfonamide (XTZ) ligand has strong interactions with the dummy atoms of the protein as shown in Fig. 6(G). The 2D interaction of the XTZ ligand

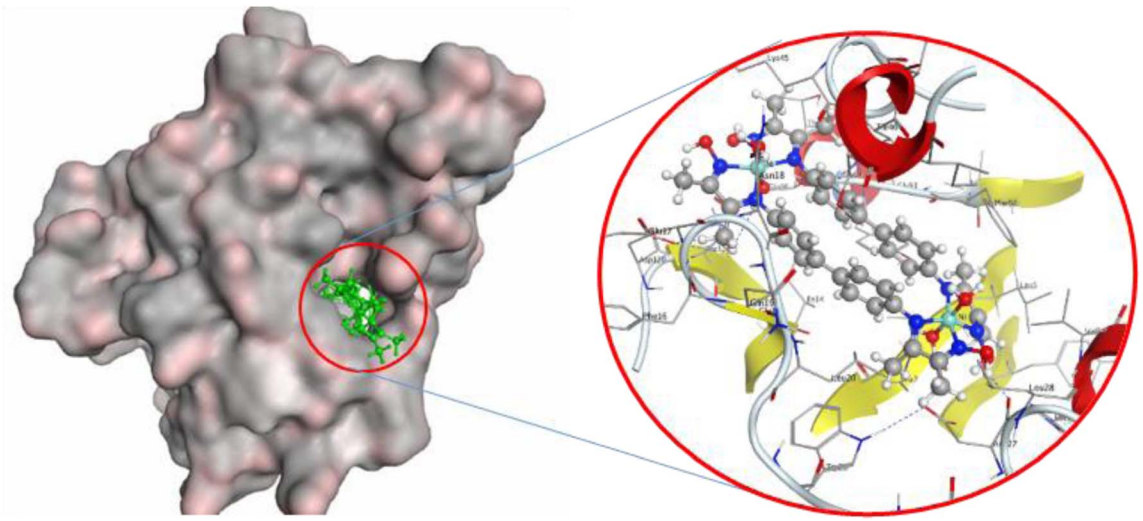

Fig. 5 3D interaction of bis-benzidinedioxime nickel(II) with DHFR pocket.

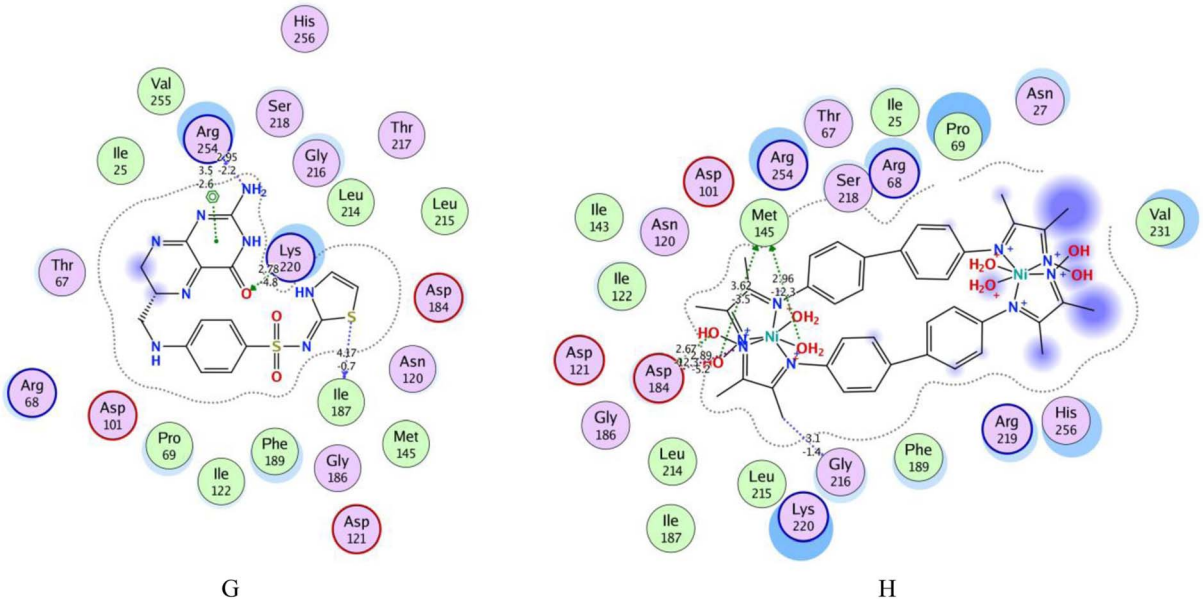

Fig. 6 2D interaction of XTZ ligand, and bis-benzidinedioxime complexes with DHPS pocket, (G) 2D interaction of the XTZ ligand with DHPS pocket. (H) 2D interaction of complex of nickel(II) with DHPS pocket respectively.

displays that the crystalline ligand XTZ formed a donor hydrogen bond by the Arg 254 with an amino group and Ile 187 with a sulfur atom at the thiazole ring; furthermore, the acceptor hydrogen bond formed between the XTZ ligand with the active site. The carbonyl group at the benzene ring has a moderately strong acceptor hydrogen bond to Lys 220. Arene–H interaction formed with the benzene ring and Arg 254. Lys 220, Gly 216, Phe 189, and Arg 68 residues are interfaced with the side chains of the XTZ ligand by Vander Waal forces.

The 2D and 3D interactions of bis-benzidinedioxime nickel(II) within the active site of DHPS are shown in Fig. 6(H) and 7. The co-crystallized bis-benzidinedioxime nickel II with 3TYE has formed four hydrogen bonds between Asp 218, Gly 216, and Met 145. An ionic bond is generated between the oxime group's oxygen atoms with Asp 18. The region around the alkyl chains in the terminal of the molecule is a hydrophobic surface in the proximity of "greasy" residues, which are appeared in light green. The polar surface of bis-benzidinedioxime nickel(II) has more closely affiliated with polar or ionic residues. The loosening of contour and the high solvent exposure of the terminal atoms indicate that the oxime and alkyl groups at the end of the ligand (right) are far out of the active site. The bis-benzidinedioxime palladium(II) showed a strong binding pattern with the DHPS enzyme. The 2D interaction palladium(II)

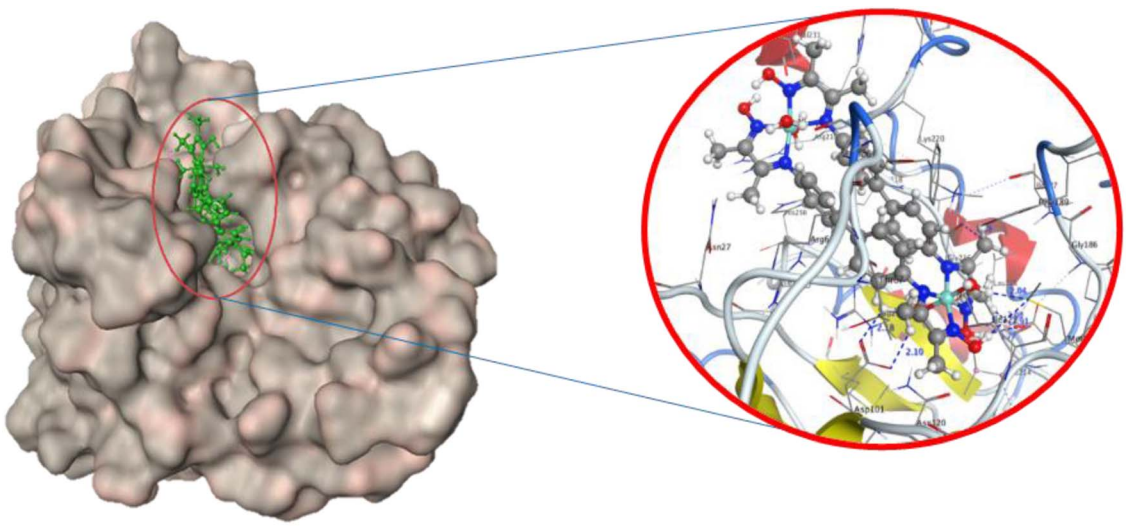

Fig. 7 3D interaction of bis-benzidinedioxime nickel(II) with DHPS pocket.

complex with an active site exhibited the ionic bond formed between the hydroxyl group and Asp 184. Both alkyl and oxime groups of complex interacted with the Asp 101, Met 145, and Gly 216 *via* donor hydrogen bonds. The rest of the amino acid residues Lys 220, Ser 221, Arg 68, Pro 69, Val 231, Arg 219, His 256, Ser 218, Arg 254, Gly 216, Asp 184, Asn 120, Ile 122, Thr 67 and Phe 189 formed Vander Waal interactions with palladium(II) complex Fig. 7ESI(I).† Losing the contour around a compound indicated that the intermediate solvent interacted with terminal atoms. The phenyl ring in bis-benzidinedioxime platinum(IV) engaged with Ser 221 by arene–H interaction, and also the platinum(IV) complex formed Vander Waal interactions with Ser 218, Arg 219, Lys 220, His 256, Ser 221, Gly 188, Pro 69, Phe 71, Phe 189, Arg 68, Arg 254 and Thr 67 Fig. 7ESI(J).† Losing the contour around a compound indicated that the intermediate solvent interacted with terminal atoms. The benzidinedioxime interacts with DHPS *via* connected arene H interaction between the phenyl group and lys 220. The amino acid residues Thr 67, Phe189, Arg 254, Ile 122, Asp 184, Asn 120, Pro 69, Lys 220, and Ser 221 interacted Vander Waal interactions with benzidinedioxime Fig. 7ESI(K).†

2D interaction of palladium(II) complex, platinum(IV), and benzidinedioxime with DHFR pocket and DHPS Pocket are available in Fig. 6ESI and 7,† respectively.

Biological activity

The synthesized ligand and complexes screened for antimicrobial activities against different bacterial species and fungi. All complexes have higher biological activities against most of the tested microorganisms than the free ligand, confirming that the transition metals increase the activity of the compounds against them.[26,49–51] The high antimicrobial activity of the complexes as compared to the benzidinedioxime might be due to their highest lipophilicity. This causes an increase in their penetration ability through the lipid membrane, which could block or inhibit the growth of the microorganism.[52–54] The nickel(II) complex showed the highest antibacterial activity against

Table 7 Antibacterial inhibition zone in mm ± standard deviation of synthesized compounds

	Diameter of the inhibition zone (mm)					
					Drugs	
Bacterial and fungi	Ni(II)	Pd(II)	Pt(IV)	L	Gentamycin	SMX–TMP
E. coli	17.3 ± 1.8	22.3 ± 2.2	0	15.0 ± 0.00	27	32
P. vulgaris	15.7 ± 0.89	10.7 ± 2.2	0	0	25	35
S. Typhimurium	16.3 ± 1.1	18.3 ± 1.1	14.0 ± 1.0	12.7 ± 1.8	26	35
PS. areuginosa	17.3 ± 11	14.0 ± 0.0	0	14.7 ± 0.4	27	0
S. aruse	17.7 ± 0.4	0	0	14.3 ± 1.6	25	33
B. Subtilis	19.0 ± 0.7	16.7 ± 2.2	19.3 ± 0.9	16.7 ± 2.2	26	21
Candida	16.3 ± 1.1	15.0 ± 0.7	13.3 ± 0.44	14.3 ± 1.1	25	33

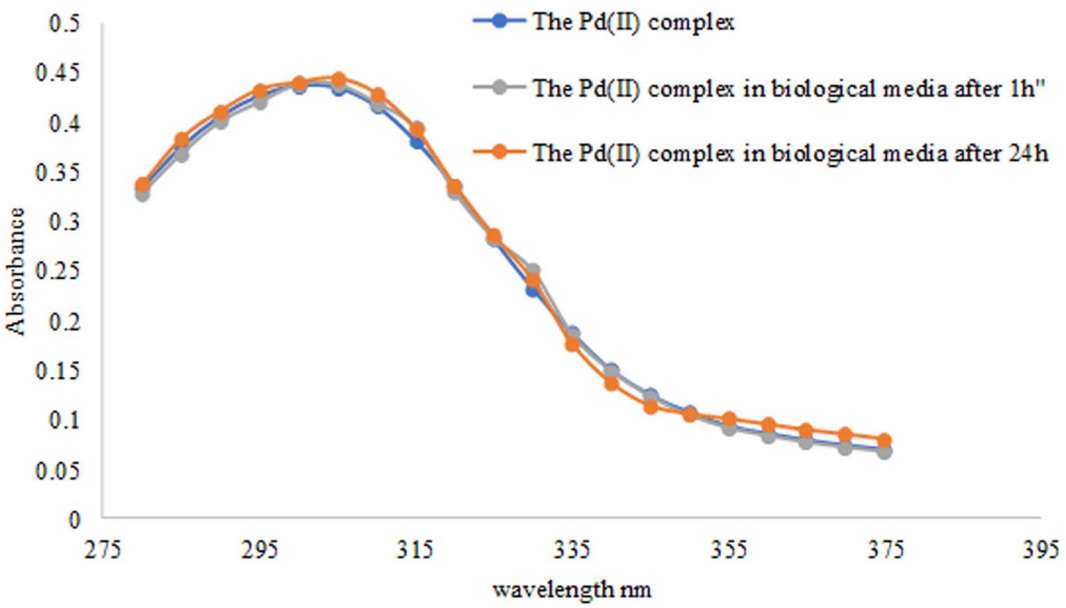

Fig. 8 Stability of bis-benzidinedioxime palladium(II) in biological media.

microorganisms of all the tested complexes. On the other hand, the platinum(IV) complex showed the lowest activity against microorganisms, as summarized in Table 7.

All synthesized complexes and a ligand exhibit a significant result against *PS. Aeruginous* than their corresponding SMX–TMP drugs[54] Table 7. The study of palladium(II) complex stability in biological media showed no difference between the three scans, the complex alone and the complex in LB media after 1 h and 24 h. These results indicated the high stability of palladium(II) in biological media Fig. 8.

Conclusion

The complex compounds were prepared and characterized using elemental analysis, ^{1}HNMR, UV-VIS spectrophotometer, scanning electron microscopy, and powder X-ray diffraction techniques. The results of spectrum techniques and powder XRD analyses deduced that the complex of bis-benzidinedioxime nickel(II) and bis-benzidinedioxime platinum(IV) have little octahedral geometry distortion. In contrast, bis-benzidinedioxime palladium(II) has square planar geometry distortion. Molecular docking studies showed that this compound had occupied both the *p*-aminobenzoic acid and pterin binding pockets of DHPS and DHFR. The antimicrobial activity study indicates that all complexes showed more activity than the ligand against the same microorganisms under identical experimental conditions. This provides supportive information and suggests using the complexes to control the selected microbial infection.

Conflicts of interest

The authors listed immediately above certify that they did not receive support from any organization for the submitted work. No funding was received to assist with the preparation of this manuscript. No funding was received for conducting this study. No funds, grants, or other support were received.

Acknowledgements

We thank professor Emadaldin Konozy, Head Department of Biotechnology, Research Center, Africa City of Technology, for his immense support during this work. Furthermore, thank Dr Babita Behera, CSIR-Indian Institute of Petroleum, Dehradun – Uttarakhand-248005, India, for the ^{1}HNMR measurement.

References

1 J. Kumar, A. Rai and V. Raj, *Org. Med. Chem. J*, 2017, **1**, 555–564.
2 S. N. Shariff, S. Saravu and D. Ramakrishna, in *Schiff Base in Organic, Inorganic and Physical Chemistry*, IntechOpen, 2022.
3 R. K. Mohapatra, P. K. Das, M. K. Pradhan, A. A. Maihub and M. M. El-Ajaily, *J. Iran. Chem. Soc.*, 2018, **15**, 2193–2227.
4 J. Anacona, Y. Pineda, A. Bravo and J. Camus, *Med. Chem.*, 2016, **6**, 467.
5 R. Nair, A. Shah, S. Baluja and S. Chanda, *J. Serb. Chem. Soc.*, 2006, **71**, 733–744.
6 M. N. Uddin, S. S. Ahmed and S. R. Alam, *J. Coord. Chem.*, 2020, **73**, 3109–3149.
7 S. A. Dalia, F. Afsan, M. S. Hossain, M. N. Khan, C. Zakaria, M.-E. Zahan and M. Ali, *Int. J. Chem. Stud.*, 2018, **6**, 2859–2867.
8 Y. Wang, X. Yu, B. Lu, W. Ye and S. Sheng, *Chem. Abstr.*, 2002, **23**, 257–301.
9 Y. Wang, B. Lu, X. Yu, W. Ye and S. Wang, *Chem. J. Internet*, 2001, **3**, 51.
10 S. Chaves-Silva, L. P. Horta, L. T. Souza, C. M. da Silva, C. S. Dohanik, G. A. Goulart, I. E. Marriel, Â. de Fátima and L. V. Modolo, *Ind. Crops Prod.*, 2020, **145**, 111995.
11 P. Ghanghas, A. Choudhary, D. Kumar and K. Poonia, *Inorg. Chem. Commun.*, 2021, **130**, 108710.
12 M. Yadav, D. Yadav, D. P. Singh and J. K. Kapoor, *Inorg. Chim. Acta*, 2022, 121300.
13 É. N. Oiye, M. F. M. Ribeiro, J. M. T. Katayama, M. C. Tadini, M. A. Balbino, I. C. Eleotério, J. Magalhães, A. S. Castro, R. S. M. Silva and J. W. da Cruz Júnior, *Crit. Rev. Anal. Chem.*, 2019, **49**, 488–509.
14 T. Akitsu, B. Miroslaw and S. Sudarsan, *Int. J. Mol. Sci.*, 2022, **23**, 10005.
15 P. Mahadevi and S. Sumathi, *Synth. Commun.*, 2020, **50**, 2237–2249.
16 A. Campos, J. Anacona and M. Campos-Vallette, *Main Group Met. Chem.*, 1999, **22**, 283–288.
17 S. Chandar, *J. Indian Chem. Soc.*, 2004, **81**, 203–206.
18 P. G. Cozzi, *Chem. Soc. Rev.*, 2004, **33**, 410–421.
19 M. Verma, S. N. Pandeya, K. N. Singh and J. P. Stables, *Acta Pharm.*, 2004, **54**, 49–56.
20 D. R. Williams, *Chem. Rev.*, 1972, **72**, 203–213.
21 S. Kumar, D. N. Dhar and P. Saxena, *J. Serb. Chem. Soc.*, 2009, **68**, 181–187.
22 O. Kahn, *Angew Chem. Int. Ed. Engl.*, 1985, **24**, 834–850.
23 L. Hua, F.-W. Zheng, H.-T. Chen, L. Wang, D.-J. Li, L. Yang, F.-J. Han, X.-Y. Duan, T.-T. Liu and W.-X. Wang, *J. Solid State Chem.*, 2021, 122463.
24 L. Rigamonti, P. Zardi, S. Carlino, F. Demartin, C. Castellano, L. Pigani, A. Ponti, A. M. Ferretti and A. Pasini, *Int. J. Mol. Sci.*, 2020, **21**, 7882.
25 B. Es-Sounni, A. Nakkabi, A. Bouymajane, I. Elaaraj, M. Bakhouch, F. R. Filali, M. El Yazidi, N. El Moualij and M. Fahim, *Biointerface Res. Appl. Chem.*, 2022, **13**, 1–14.
26 H. Kargar, A. A. Ardakani, M. N. Tahir, M. Ashfaq and K. S. Munawar, *J. Mol. Struct.*, 2021, **1233**, 130112.
27 K. Turecka, A. Chylewska, A. Kawiak and K. F. Waleron, *Front. Microbiol.*, 2018, **9**, 1594.
28 B. Geeta, K. Shravankumar, P. M. Reddy, E. Ravikrishna, M. Sarangapani, K. K. Reddy and V. Ravinder, *Spectrochim. Acta, Part A*, 2010, **77**, 911–915.
29 T. Y. Fonkui, M. I. Ikhile, D. T. Ndinteh and P. B. Njobeh, *Trop. J. Pharm. Res.*, 2018, **17**, 2507–2518.
30 E. Khan, *ChemistrySelect*, 2021, **6**, 3041–3064.
31 R. A. Azzam, R. E. Elsayed and G. H. Elgemeie, *ACS Omega*, 2020, **5**, 10401–10414.

32 H. Lade and J. S. Kim, *Antibiotics*, 2021, **10**, 398.
33 M. K. Yun, Y. Wu, Z. Li, Y. Zhao, M. B. Waddell, A. M. Ferreira, R. E. Lee, D. Bashford and S. W. White, *Science*, 2012, **335**, 1110–1114.
34 C. Capasso and C. T. Supuran, *J. Enzyme Inhib. Med. Chem.*, 2014, **29**, 379–387.
35 M. Graffner Nordberg, K. Kolmodin, J. Aqvist, S. F. Queener and A. Hallberg, *J. Med. Chem*, 2001, **44**, 2391–2402.
36 A. Wrobel, K. Arciszewska, D. Maliszewski and D. Drozdowska, *J. Antibiot.*, 2020, **73**, 5–27.
37 H. Seeley and P. Van Denmark, *A laboratory manual of microbiology*, Taraporewala Sons and Co., Mumbai, 1975, p. 55.
38 Z. A. Saleh and D. K. Kafi, *Phys. Chem.*, 2016, **6**, 49–56.
39 K. Buldurun, N. Turan, A. Savcı and N. Colak, *J. Saudi Chem. Soc.*, 2019, **23**, 205–214.
40 M. Mishra, K. Tiwari, A. K. Singh and V. P. Singh, *Polyhedron*, 2014, **77**, 57–65.
41 B. Shafaatian, A. Soleymanpour, N. K. Oskouei, B. Notash and S. A. Rezvani, *Spectrochim. Acta, Part A*, 2014, **128**, 363–369.
42 J. W. Akitt and B. E. Mann, *NMR and Chemistry: An Introduction to Modern NMR Spectroscopy*, CRC Press, 2017.
43 N. S. Gwaram, H. M. Ali, H. Khaledi, M. A. Abdulla, A. H. A. Hadi, T. K. Lin, C. L. Ching and C. L. Ooi, *Molecules*, 2012, **17**, 5952–5971.
44 N. E. Jacobsen, *NMR Spectroscopy Explained: Simplified Theory, Applications and Examples for Organic Chemistry and Structural Biology*, John Wiley & Sons, 2007.
45 M. Babinský, K. Bouzková, M. Pipíška, L. Novosadová and R. Marek, *J. Phys. Chem. A*, 2013, **117**, 497–503.
46 Y. M. Dikova, D. S. Yufit and J. G. Williams, *Inorg. Chem.*, 2023, **62**, 1306–1322.
47 A. D. Aputen, M. G. Elias, J. Gilbert, J. A. Sakoff, C. P. Gordon, K. F. Scott and J. R. Aldrich-Wright, *Molecules*, 2022, **27**, 7120.
48 M. Novák, C. Foroutan-Nejad and R. Marek, *Phys. Chem. Chem. Phys.*, 2015, **17**, 6440–6450.
49 L. H. Abdel-Rahman, R. M. El-Khatib, L. A. Nassr, A. M. Abu-Dief and F. E.-D. Lashin, *Spectrochim. Acta, Part A*, 2013, **111**, 266–276.
50 M. Neelakantan, S. Marriappan, J. Dharmaraja, T. Jeyakumar and K. Muthukumaran, *Spectrochim. Acta, Part A*, 2008, **71**, 628–635.
51 U. El-Ayaan and A.-M. Alaa, *Eur. J. Med. Chem.*, 2005, **40**, 1214–1221.
52 Z. H. Chohan and M. Praveen, *Appl. Organomet. Chem.*, 2001, **15**, 617–625.
53 Z. H. Chohan and M. Praveen, *Appl. Organomet. Chem.*, 2000, **14**, 376–382.
54 A. Beheshti, F. Hashemi, F. Behavndi, M. Zahedi, M. Kolahi, H. Motamedi and P. Mayer, *Int. J. Biol. Macromol.*, 2017, **104**, 1107–1123.